DOI:10.1190/segam2020-3411920.1

Near-surface velocity uncertainty estimation through Bayesian tomography approach

Anton Egorov and Pavel Golikov, Aramco Research Center Moscow; Ilya Silvestrov and Andrey Bakulin, EXPEC Advanced Research Center, Saudi Aramco

Summary

The accuracy of seismic structural interpretation strongly depends on the velocity model used for the imaging, particularly on the near-surface velocities. In the standard processing workflows used in exploration geophysics, the near-surface velocities are obtained by deterministic first arrival tomography, which limits the options for structural uncertainty estimation. We demonstrate the benefits of hierarchical transdimensional Bayesian first arrival tomography on an exploration-scale 2D scenario. Such a tomography yields multiple models of the near-surface that fit the observed traveltimes. In addition to the velocity uncertainty, we analyze the static corrections associated with these velocities to obtain an estimated structural uncertainty for two different seismic acquisition geometries.

Introduction

Complex near-surface geology is one of the most challenging issues for land seismic data processing and interpretation (Robinson and Al-Husseini, 1982). The accuracy of seismic imaging strongly depends on the accuracy of the near-surface velocity model (Bakulin et al., 2017). One of the main instruments for the near-surface velocity reconstruction is the refraction traveltime tomography, which relies on the arrival times of diving/refracted waves (Zhang and Toksöz, 1998). This model is then either used for the computation of static corrections or directly embedded into the velocity model for seismic migration from topography.

Seismic tomography is often conducted in a deterministic manner, yielding a single velocity model, which depends on the user-defined parameters (e.g., regularization coefficients) and does not provide any direct estimates of uncertainty. There are numerous ways to estimate the uncertainty of tomography, which are often applied in the seismological community (Rawlinson et al., 2014) and less often in oil and gas exploration (Osypov et al., 2013). One of the options is the Bayesian framework, which allows one to obtain numerous models that fit the observed traveltimes and compute various statistics from these models. Such techniques have been applied to seismological datasets for different subsurface models and survey geometries (Bodin et al., 2012; Ryberg and Haberland, 2018). Here, we apply 2D Bayesian first arrival tomography for near-surface velocity estimation in a seismic exploration scenario, specifically to imaging low-relief structures in the presence of complex near surface (Bakulin et al., 2017). In addition to evaluating the velocity uncertainty, we attempt to propagate this uncertainty through the seismic processing workflow by estimating the errors of static corrections. Low-relief structures typically have vertical closures of less than 30 ms, and the correct structural imaging, in this case, requires the near-surface velocities and long-wavelength static corrections to be estimated with high accuracy.

Method

We apply a 2D hierarchical reversible-jump Markov Chain Monte Carlo (rj-MCMC) method by Bodin et al. (2012). We parameterize the subsurface by N unstructured points, each of the points is defined by the velocity value v_i and coordinates x_i and z_i, all of which are the parameters updated by the algorithm. The velocity model in the whole domain is computed from this set of points by linear interpolation within triangles. Traditionally, Voronoi tessellation has been used for this purpose; however, linear interpolation within triangles was found to be more effective for smooth velocity models and refraction geometry by Ryberg and Haberland (2018). Two additional parameters are the number of points in the model N (a small number in comparison to the number of regular grid cells) and the standard deviation of picking noise σ_n, which is also estimated in the hierarchical Bayesian framework. Here, we assume that the picking errors have Gaussian distribution and are uncorrelated.

We use multiple noninteracting Markov chains. Each chain gets an initial model from the priors. We use wide priors: we allow the velocities to change from 1,000 to 8,000 m/s and the number of parameters from 21 to 241. At each step of the chain, either a new position or velocity is proposed for one of the points, or the birth/death of one of the points happens, or σ_n changes. The new model is then accepted or rejected by comparing its traveltime misfit to the misfit of the current model. For the comparison, a version of Metropolis-Hastings acceptance criterion modified for the reversible-jump method (Green, 1995) is used. The criterion sometimes may accept a model with the larger misfit, which results in a random-walk like behavior of the chain and allows the chain to continue sampling from the posterior model distribution instead of converging to a single model. After collecting enough chains, we analyze the accepted models and estimate the velocity uncertainty by computing the average, various moments (e.g., standard deviation) or by directly looking at velocity distributions for each of the points in the subsurface. We compute the traveltimes with an eikonal solver. We do a full eikonal computation at every step of the algorithm, in contrast to Bodin et al. (2012), who use inner and outer loops, computing rays in the outer loop and updating the

model with fixed rays in the inner loop. This takes extra time but allows us to avoid the tuning of the inner loop length.

To get an estimate of the uncertainty of static corrections associated with the velocity uncertainty, we calculate static corrections from each of the near-surface velocity models sampled by the rj-MCMC and analyze their influence on a low-relief structure with the closure of 30 ms.

Example – velocity uncertainty

For this study, we use a simple 1D gradient velocity model with two near-surface anomalies (Figure 1a). The underlying grid cell size for eikonal computations is 50 x 50 m. The sources and receivers are located on the surface of the model with 200 m and 100 m spacings, respectively. We compute the traveltimes for this acquisition configuration. We then add zero-mean Gaussian noise with 5 ms standard deviation to these traveltimes. The hierarchical Bayesian algorithm is supposed to reconstruct the value of noise standard deviation together with the subsurface models.

We run 56 rj-MCMC chains, collecting 300,000 accepted samples for each of the chains. Then we disregard the first 250,000 samples as burn-in and thin the chains, picking every 100th accepted sample. The misfit plots for all the chains are displayed in Figure 2.

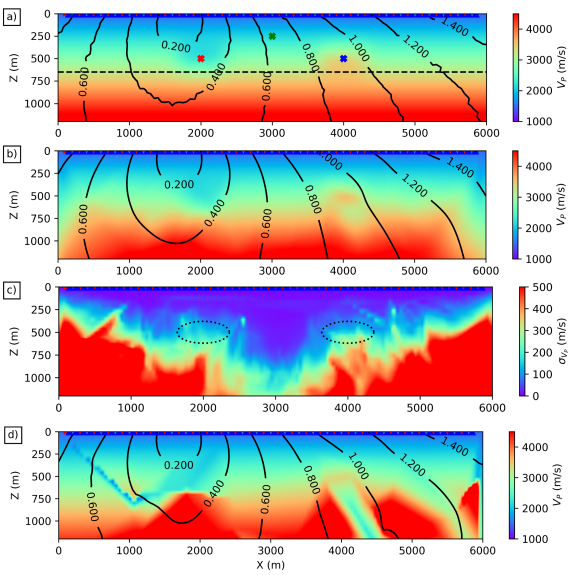

Figure 1: True velocity model (a), average model over all chains (b), estimated standard deviation (c) and an example stochastic realization from one of the chains (d). Traveltimes in seconds for one of the shots are displayed over the models; the true traveltimes contain the added Gaussian noise. The dashed line in (a) shows the datum used for computation of static corrections shown below. Crosses show the points analyzed in Figure 3; dotted ellipses on the standard deviation plot outline the velocity anomalies.

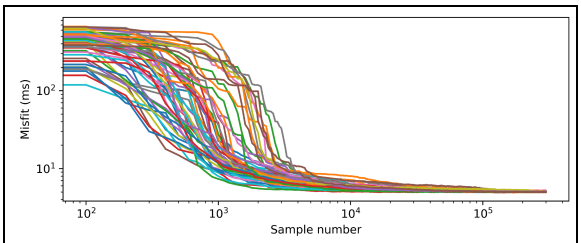

Figure 2: Root-mean square traveltime misfit for all computed chains. Note the logarithmic scale for both axes. The first 250,000 samples are discarded from further analysis.

Using the 500 models from each of the chains remaining after burn-in removal and thinning, we compute the average velocity and standard deviation (Figures 1b and 1c). An example of one model extracted from the chains is displayed in Figure 1d. The average velocity model for this case approximates the correct velocity model quite well. The standard deviation has artifacts related to the parameterization, but it still shows the main trends – the velocity error increases with depth and is large on the sides of the model – the areas not illuminated by the survey geometry. As expected, the area of the most certain velocity estimation is following the good ray coverage region.

The Bayesian framework also allows one to examine the velocity distributions for each point in the model. Figure 3a-c shows the velocity distributions for the three points displayed in Figure 1a with matching colors. We observe that the velocity uncertainty increases with depth. The velocity distribution for a high-velocity anomaly (blue) is slightly skewed with regards to the true value.

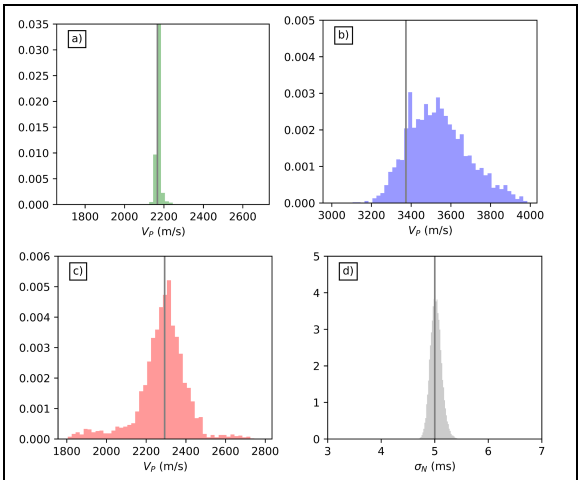

Figure 3: Posterior velocity distributions for three points indicated in Figure 1a (a-c) and the posterior distribution of picking error standard deviation (d). True values are shown by vertical grey lines. Note that each horizontal axis spans 1000 m/s in (a-c).

Figure 3d shows the histogram of the noise level estimated by the method. The maximum of the histogram is close to the picking error we used for the modeled traveltimes. The Gaussian uncorrelated noise model may be too simple for the real data inversion. In principle, hierarchical Bayesian formulation allows more sophisticated noise models.

Example – the uncertainty of static corrections

Using these models, we attempt to analyze the uncertainty in the reconstruction of a low-relief structure. We use the standard assumptions involved in the model of static corrections, such as vertical-ray approximation (Cox, 1999). For illustration purposes, we consider a zero-offset geometry and directly map the static corrections computed for each surface location onto the low-relief structure. We pick a low-relief structure with the closure of 30 ms. The structure perturbation caused by velocity anomalies is shown as a red line in Figure 4a. True statics provide a perfect reconstruction of the reflector (green line in Figure 4a). For the calculation of statics, we used a flat datum at a depth of 650 m and a suitable replacement velocity. Then, we calculate the static corrections using the near-surface models obtained by tomography. First, we compute the static corrections from the average velocity model over all the chains and display the reconstructed horizon as a blue line in Figure 4a. While this reconstruction preserves the geometrical shape of the low-relief structure, we observe some oscillations with a maximum deviation of 7 ms. It is also important to note that the quality of the reconstruction depends on the traveltime picking error, which is quite optimistic in our example. Using a higher error would lead to a less accurate result.

To get an estimate of the error in horizon locations, we take all the stochastic models generated by the algorithm and compute the static corrections from each of these models. It is important to note that all the analyzed models have low traveltime misfits from 4.9 to 5.3 ms, which is close to the 5 ms picking error. So, all these models are approximately equal in terms of probability. As some of those models are less smooth (e.g., Figure 1d), the associated reflector reconstructions may be oscillating. Dotted black lines in Figure 4 show a few examples of the horizon reconstruction with those statics. We also compute posterior probability density functions (PDFs) of possible horizon reconstructions at every point along the horizon and plot these histograms as a background in Figure 4a. Note that the horizon reconstruction obtained with the average model (blue line) does not always coincide with the maximum of the PDFs. This is related to the fact that the PDF maximum represents the mode of the distribution, which can differ from the average (in our case, the average statics over all models are almost equal to the statics computed from the average velocity). We note that below the low-velocity anomaly, the PDFs are less focused, and the horizon geometries obtained

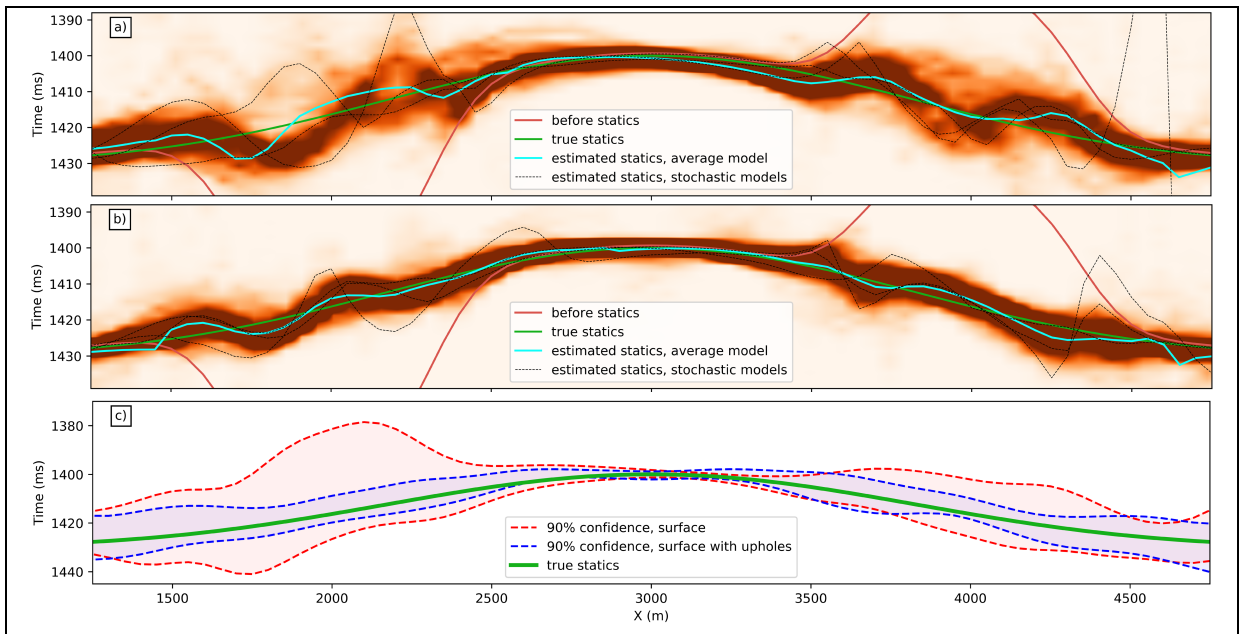

Figure 4: (a) A low-relief structure before static corrections (red), after true static corrections (green), after static corrections generated from the average tomography model (blue) and three versions of reflector reconstruction computed from different low-misfit models in the chain (dotted black). A set of 1D histograms of possible horizon reconstruction for every X is displayed as a background; (b) same as (a), but with two wells added in the acquisition geometry; (c) comparison of 90% confidence intervals of reflector locations for two different types of acquisition.

from the stochastic models (dotted black lines) tend to oscillate more comparing to the high-velocity anomaly. Such behavior can be attributed to the larger uncertainty of first arrival tomography problem in the presence of low-velocity structures and velocity inversions (Liu et al., 2010); however, this effect is not as prominent here as we expected.

Example - reducing the uncertainty by vertical arrays

To study the near-surface velocities, seismic receivers can also be placed in shallow wells and be used in conjunction with the surface receivers. Smart DAS geometry used by Bakulin et al. (2017) is an example of such an on-demand acquisition geometry enhancement. Bayesian tomography can provide an understanding of the added value brought by the vertical receiver arrays in terms of the velocity uncertainty. To estimate the reduction of uncertainty provided by such acquisition, we repeat the experiment for a different acquisition geometry. We use the same sources, but we add two vertical receiver arrays directly in the centers of the velocity anomalies (Figure 5a). The wells have horizontal coordinates of 2,000 and 4,000 m; maximum receiver depth is equal to 650 m (the datum depth). The vertical arrays record all the shots in the survey.

Figure 5 shows the average velocity model and the standard deviation for this geometry. While the average velocity is similar to the one obtained with surface receivers only, the standard deviation of the velocities is significantly lower. This reduction of errors is also clearly seen in Figure 4b, which shows the estimation of uncertainty of static corrections obtained using the vertical arrays in conjunction with the surface receivers. The increase in structural accuracy manifests itself in the improved reconstruction of the reflector (blue line in Figure 4b). The PDFs of possible reflector locations have narrower maxima, which more closely follows the true geometry of the low-relief structure. Analyzing the 90% confidence intervals shown in Figure 4c, we can observe that the vertical receiver arrays decrease the uncertainty below the anomalies – for example, the 90% confidence interval shrinks from more than 40 ms to 15 ms just below the low-velocity anomaly.

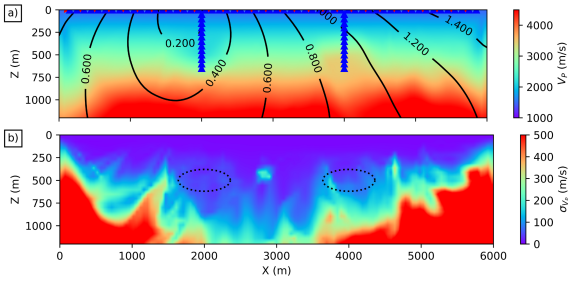

Figure 5: Average velocity model over all the chains for the acquisition with vertical receiver arrays (a) and the estimated standard deviation (b). Traveltimes in seconds for one of the shots are displayed over the model. Acquisition geometry is shown in (a).

Discussion

The main drawback of the Bayesian seismic tomography is its computational cost. In the case of our 2D example, one chain runs for approximately 30 hours on one Intel Xeon 2.6 GHz processor core. While a 3D example was demonstrated by Zhang et al. (2018), it is still unclear whether rj-MCMC tomography is feasible for exploration-scale 3D seismic, as the method's complexity increases exponentially with the number of parameters. It was recently shown by Fichtner et al. (2019) that an alternative MCMC method, Hamiltonian Monte Carlo, may facilitate the transition to 3D.

Another critical point is that we use static corrections as an estimate of the structural uncertainty. While still being widely used in practice, static corrections are a simple approximation. A more elaborate study would require conducting full-scale migrations of a synthetic dataset with the numerous velocity models generated by the Bayesian tomography and analyzing the uncertainty in the low-relief structure geometry on these migration results.

Conclusions

The Bayesian framework allows uncertainty estimation for the seismic tomography. We conduct a test of Bayesian first arrival tomography for a 2D exploration-scale near-surface refraction model. The tomography successfully estimates the reference velocity model and the velocity uncertainty at each point of the model. It is important to note that no initial model is needed for the estimation – we only used very wide uniform priors for the unknowns.

These uncertainties are then used to estimate the error in static corrections and associated structural uncertainty for a low-relief structure with the closure of 30 ms for two different seismic acquisition geometries. The results of the tomography suggest that the receivers in the shallow wells significantly decrease the velocity uncertainty and, consequently, structural uncertainty. As the vertical receiver arrays, unlike conventional upholes, record all the sources in the survey, they decrease the velocity uncertainty not only in the well, but also around it. It is also important to note that one may use such an analysis before acquisition in order to pick the locations of the vertical arrays that decrease the uncertainty most effectively.

Acknowledgments

The authors would like to thank T. Zharnikov and M. Al-Ali (Aramco Research Center in Moscow) for productive discussions on this research topic.

REFERENCES

Bakulin, A., P. Golikov, R. Smith, K. Erickson, I. Silvestrov, and M. Al-Ali, 2017, Smart DAS upholes for simultaneous land near-surface characterization and subsurface imaging: The Leading Edge, **36**, 1001–1008, doi: https://doi.org/10.1190/tle36121001.1.

Bodin, T., M. Sambridge, N. Rawlinson, and P. Arroucau, 2012, Transdimensional tomography with unknown data noise: Geophysical Journal International, **189**, 1536–1556, doi: https://doi.org/10.1111/j.1365-246X.2012.05414.x.

Cox, M., 1999, Static corrections for seismic reflection surveys: SEG.

Fichtner, A., A. Zunino, and L. Gebraad, 2019, Hamiltonian Monte Carlo solution of tomographic inverse problems: Geophysical Journal International, **216**, 1344–1363, doi: https://doi.org/10.1093/gjihttps://doi.org//ggy496.

Green, P. J., 1995, Reversible jump Markov chain Monte Carlo computation and Bayesian model determination: Biometrika, **82**, 711–732, doi: https://doi.org/10.1093/biomethttps://doi.org//82.4.711.

Liu, H., H. Zhou, W. Liu, P. Li, and Z. Zou, 2010, Tomographic velocity model building of the near surface with velocity-inversion interfaces: A test using the Yilmaz model: Geophysics, **75**, no. 6, U39–U47, doi: https://doi.org/10.1190/1.3502665.

Osypov, K., Y. Yang, A. Fournier, N. Ivanova, R. Bachrach, C. E. Yarman, Y. You, D. Nichols, and M. Woodward, 2013, Model-uncertainty quantification in seismic tomography: method and applications: Geophysical Prospecting, **61**, 1114–1134, doi: https://doi.org/10.1111/1365-2478.12058.

Rawlinson, N., A. Fichtner, M. Sambridge, and M. K. Young, 2014, Seismic tomography and the assessment of uncertainty, in R. Dmowska, ed., Advances in geophysics, **55**, Elsevier, 1–76.

Robinson, D., and M. I. Al-Husseini, 1982, Technique for reflection prospecting in the Rub' Al-Khali: Geophysics, **47**, 1135–1152, doi: https://doi.org/10.1190/1.1441377.

Ryberg, T., and C. Haberland, 2018, Bayesian inversion of refraction seismic traveltime data: Geophysical Journal International, **212**, 1645–1656, doi: https://doi.org/10.1093/gjihttps://doi.org//ggx500.

Zhang, J., and M. Toksöz, 1998, Nonlinear refraction traveltime tomography: Geophysics, **63**, 1726–1737, doi: https://doi.org/10.1190/1.1444468.

Zhang, X., A. Curtis, E. Galetti, and S. de Ridder, 2018, 3-D Monte Carlo surface wave tomography: Geophysical Journal International, **215**, 1644–1658, doi: https://doi.org/10.1093/gjihttps://doi.org//ggy362.